A Strain-Based Health Indicator for the SHM of Skin-to-Stringer Disbond Growth of Composite Stiffened Panels in Fatigue

Milanoski, Dimitrios; Galanopoulos, Georgios; Broer, Agnes; Zarouchas, Dimitrios; Loutas, Theodoros

DOI
10.1007/978-3-030-64594-6_61

Publication date
2021

Document Version
Final published version

Published in
European Workshop on Structural Health Monitoring - Special Collection of 2020 Papers - Volume 1

Citation (APA)
Milanoski, D., Galanopoulos, G., Broer, A., Zarouchas, D., & Loutas, T. (2021). A Strain-Based Health Indicator for the SHM of Skin-to-Stringer Disbond Growth of Composite Stiffened Panels in Fatigue. In P. Rizzo, & A. Milazzo (Eds.), *European Workshop on Structural Health Monitoring - Special Collection of 2020 Papers - Volume 1* (pp. 626-635). (European Workshop on Structural Health Monitoring - Special Collection of 2020 Papers - Volume 1; Vol. 127). Springer. https://doi.org/10.1007/978-3-030-64594-6_61

A Strain-Based Health Indicator for the SHM of Skin-to-Stringer Disbond Growth of Composite Stiffened Panels in Fatigue

Dimitrios Milanoski[1(✉)], Georgios Galanopoulos[1], Agnes Broer[2], Dimitrios Zarouchas[2], and Theodoros Loutas[1]

[1] Applied Mechanics Laboratory, Department of Mechanical Engineering and Aeronautics, University of Patras, 26504 Rio, Greece
d.milanoski@g.upatras.gr
[2] Structural Integrity and Composites Group, Faculty of Aerospace Engineering, Delft University of Technology, Kluyverweg 1, 2629HS Delft, The Netherlands

Abstract. Real-time Structural Health Monitoring (SHM) of aeronautical structural components is a technology persistently investigated the last years by researchers and engineers to potentially reduce the cost and/or implementation of scheduled maintenance tasks. To this end, various types of sensors have been proposed to serve this role, e.g. piezoelectric, acoustic emission, and strain sensors. In the present paper, a strain-based SHM methodology is proposed for skin/stringer disbond propagation health monitoring. Fiber-optic strain sensors with engraved Bragg gratings are utilized in order to evaluate the propagation of artificially-induced disbonds at single-stringered composite panels. The specimens are subjected to a block loading compression-compression fatigue spectrum. Longitudinal static strains are periodically acquired during quasi-static loadings every 500 cycles. A Health Indicator (HI), based on strains received from the stringer's feet, is proposed and utilized to monitor the disbond growth. The evolution of this indicator is experimentally monitored throughout the lifespan of the specimens. The present paper verifies and consolidates via actual fatigue experiments the potential of the proposed static-strain based HI developed from numerical data in our previous work.

Keywords: Strain-based SHM · Post-buckling · Composite stiffened panels · Skin-to-stringer disbond growth · Fiber Bragg grating sensors · Fatigue testing

1 Introduction

Composite stiffened panels represent a significant proportion of modern airframe structures. Generally, the skin-to-stringer interfaces of stiffened panels are prone to the development of unseen damages as they form regions of intense stress concentrations at their edges. Moreover, unforeseen events such as foreign object impacts (e.g. tool drops) may also jeopardize the integrity of these critical areas. To this end, researchers develop Structural Health Monitoring (SHM) methodologies in an attempt to identify, localize and quantify the severity of such structural defects [1]. Recently, a tendency is being intensified towards applying the aforementioned SHM levels during operational

P. Rizzo and A. Milazzo (Eds.): EWSHM 2020, LNCE 127, pp. 626–635, 2021.
https://doi.org/10.1007/978-3-030-64594-6_61

conditions. Condition-based maintenance (CBM) aims to substitute the current periodic ground inspections with a real-time SHM evaluation via a permanently installed network of sensors [2]. An emerging category of sensors in this direction is fiber Bragg grating sensors (FBGs), a specific subcategory of fiber optic sensors (FOS), capable of measuring static and dynamic strains.

In the literature, limited studies have been developed on monitoring fatigue damage propagation, based on strain readings, oriented towards aeronautical/aerospace applications. Studies of various structural complexities can be found, from coupon level [3] or structural elements [4] to larger scale of structural components [5, 6]. A prominent experimental evaluation of the interfacial skin/stringer fatigue disbond progression can be found in Ref. [7], for the case of a hat-stiffened composite panel. A plethora of nondestructive testing (NDT) techniques was utilized, such as in-situ ultrasonic inspection (UT), passive thermography, and digital image correlation (DIC) in order to continuously monitor the disbond growth. Feng et al. [8] investigated the effect of fatigue loading on impact-induced damages of composite multi-stiffened panels. Furthermore, several works provide a deeper insight on various aspects which affect the behavior of composite stiffened panels subjected to post-buckling axial compression [9–14].

The present work implements a strain-based SHM methodology that exploits static strains acquired via surface mounted FBGs. In order to demonstrate more realistic operational conditions, and at the same time achieve gradual propagation of structural damage, we go beyond static testing and subject a composite single-stiffened panel to block loading compression-compression (C-C) fatigue. The present strain-based methodology leverages on static strains acquired during quasi-static (QS) test intervals throughout the test span. The limitations that arise due to the intrinsic dependency of strains on load, are tackled using a specially designed Health Indicator (HI) [15]. The robustness of the specific HI is investigated during the testing procedure and its sensitivity to disbond propagation is checked. Moreover, evidence of the damage extent is acquired from in-situ NDT, using a phased-array ultrasound camera. The promising results of this work empower the consolidation of a reliable SHM system operating with real-time influx of data.

2 Test Article and Experimental Campaign

2.1 Specimen Fabrication

For the purposes of this work, composite single-stringer flat panels were fabricated by OPTIMAL Structural Solutions Lda (Portugal). The skin is co-cured with a T-section stringer as depicted in Fig. 1b. Both skin and stringer are made of a graphite-epoxy continuum fiber-reinforced prepreg IM7/8552; the skin consists of 14 layers with ply orientation $[45/-45/0/45/90/-45/0]_s$ and the stringer is formed with a 10-layer layup $[45/-45/0/45/-45]_s$. In order to ensure uniform transmission of the loads to the panel, two 30 mm-thick cast-tabs, made of an epoxy casting resin EPO 5019 of Axson Technologies®, were used at the two ends of the panel as shown in Fig. 1b. The free length of the panel, i.e. between the casted regions of the tabs, is 240 mm. In total, two

defected specimens which contain a 30-mm artificial disbond at the skin/stringer interface were fabricated, by inserting Teflon amidst the two parts prior to curing process.

2.2 Experimental Campaign

The composite stiffened panels were subjected to blocks of constant amplitude C-C fatigue load with an R-ratio of 10 and testing frequency $f = 2$ Hz. The load amplitudes sequence and the rest of the operational characteristics are analytically presented in Table 1. Acquisition of the static strains, for L1_22, was enabled during a QS interval test every 500 fatigue cycles (N_f) as it is schematically depicted in Fig. 1a. The load range of each QS test was initiating from −0,5 kN up to maximum compressive load (P_{max}) with a constant displacement rate of 0.5 mm/min. Specimen L1_22 was tested in the facilities of University of Patras – Applied Mechanics Lab using a servohydraulic Instron 8802 test machine whilst L1_23 in TU Delft – Aerospace Structures and Materials Lab using an MTS test machine, with load capacities ±250 kN and ±500 kN respectively. Moreover, every QS interval for L1_23 was conducted in a load range starting from minimum (P_{min}) compressive load up to the maximum.

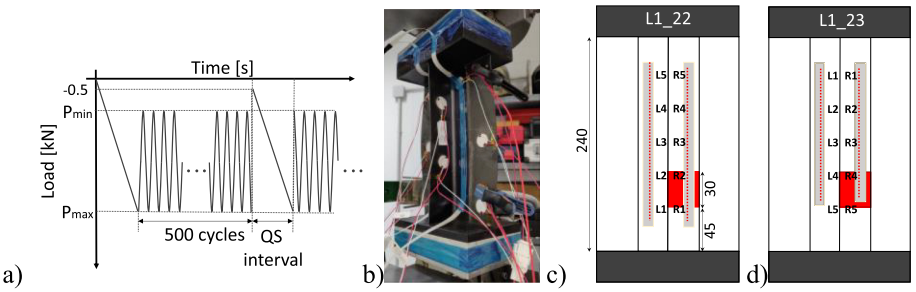

Fig. 1. a) Schematic representation of the test machine's programme, b) fully-sensorized specimen during QS compression and positions of disbond & FBGs for c) L1_22 and d) L1_23.

The specimens were sensorized in both stringer feet with a SMARTape® (see Fig. 1b), i.e. a commercial glass-epoxy tape provided by SMARTEC SA (Switzerland) which accommodates two FOS. One optical fiber operates under the principles of distributed sensing technique while the second is an FBG-based fiber having five (5) gratings along its length, with a 20-mm spacing to each other. The sensor tapes were mounted to the surface of the stringer's feet via a secondary bonding technique. A Griltex® copolyimide flexible adhesive was used to adhere the tape to the test article. Acquisition of the FBG strains was achieved using a 2-channel Micron Optics Inc. SM130 industrial grade dynamic interrogator with recording capabilities up to 1 kHz. During the QS tests, the acquisition frequency was set equal to 5 Hz. The interrogation serves the operational principle of FBGs and it is based on acquiring the reflected spectrum by the inscribed gratings. Based on the characteristics of the grating (e.g.

grating period Λ_B) the reflected light travels with the Bragg wavelength according to the Bragg equation:

$$\lambda_B = 2n_{eff}\Lambda_B \tag{1}$$

where n_{eff} is the effective refractive index and Λ_B the grating period. Whenever the optical fiber is stretched or compressed due to mechanical deformation of the monitored host material, leads to modification of the effective refractive index and the Bragg period, and subsequently to a shift on the wavelength as follows:

$$\Delta\lambda_B/\lambda_B = (1-p)\varepsilon_{11} \tag{2}$$

where p is the photo-elastic coefficient and ε_{11} is the induced longitudinal strain. Supplementary, there is also a thermal term in Eq. (2) associated to the thermal elongation of the fiber, but it was not accounted for in the current case study as the temperature did not change during the test. In Fig. 1b piezoelectric and acoustic emission sensors are also visible, which are not incorporated in the framework of the present strain-oriented methodology.

Table 1. Specifications of the fatigue test and the defected specimens.

Specimen	Damage location[a]	Max. load	R-ratio	f	Failure cycles
L1_22	¾ of stringer foot	−35 kN (10k cycles)	10	2 Hz	345k
		−39 kN (10k cycles)			
		−45 kN (10k cycles)			
		−50 kN (170k cycles)			
		−55 kN (85k cycles)			
		−60 kN (60k cycles)			
L1_23	¾ of stringer foot	−50 kN (100k cycles)	10	2 Hz	438k
		−60 kN (338k cycles)			

[a]Measuring from top tab.

3 Assessment of Skin-to-Stringer Growth

3.1 Static Strains Acquisition

The strain histories throughout the test span are presented in Fig. 2. Particularly, the FBG strains recorded at P_{max} of every QS test are depicted. For the L1_22 test article, sensor R5 was persistently recording low strains and we deduce that its bonding to the surface has been compromised. During the initial 30 k fatigue cycles, the relevant strains acquired at three different P_{max} levels, i.e. −35, −39 and −45 kN, present minor deviation as the fatigue progresses. A clear indication of the load effect (i.e. the increase of P_{max} in each block) is the stepped behavior of the induced static strains (Fig. 2a). When P_{max} is raised to −50 kN, an observed variation in the strain readings is developed, intensified in sensor R1 which is located in the vicinity of the disbond. This

observation can be attributed to a possibly increase of the disbonded area, as the newly developed surfaces would affect the sensor in their vicinity and in turn its readings. Only sensor R1 was directly above the disbonded region whilst R2 was lying outside the disbond. L1_23 initiated to operate with a nominal $P_{max} = -50$ kN. Here, we can observe a rapid monotonic drop of the measured (maximum) strain of each QS interval. This mutual evidence from both specimens led to the notion that, within the range of loads [−50, −45) kN, the 30-mm disbond has initiated growing, which resulted to the strain variations with respect to the evolution of the cycles. Both specimens buckled following the pattern of the 1st buckling mode shape, forming a single half-wave along their skin sides (see Fig. 1b) but with an opposite way to each other. This means that the induced curvature along each skin side of L1_22 is formed by an inverted way with respect to L1_23. Besides of the direct visual validation, this can be indirectly estimated if we notice that the central FBGs, i.e. R2, R3 and R4, present higher post-buckling strains from those of R1 and R5 on L1_23 whilst the opposite observation can be made for the case of L1_22. Maximum strains belonging to the left foot are not shown, but it should be noted that they presented almost negligible deviation to their values (per P_{max} level). This is a rather obvious observation, as they seem to be unaffected by the artificially-induced damage. Finally, since we do not have indirect validation of the disbond propagation for the case of L1_23, the strains are presented only for the first block, namely up to $N_f = 1 \times 10^5$.

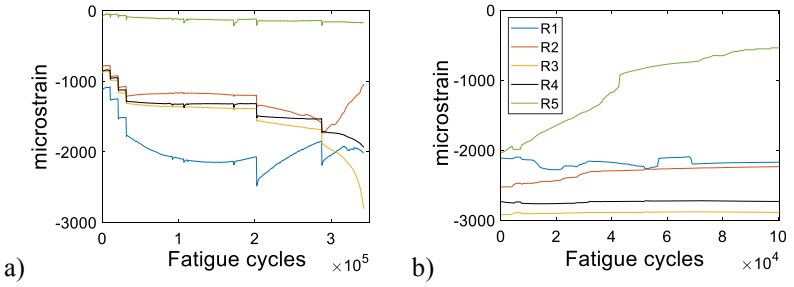

Fig. 2. Maximum FBG strains for a) L1_22 and b) L1_23 along the disbonded foot. (Similar legend for both figures)

3.2 In-Situ C-Scan Inspection

In order to enhance the SHM approach with in-situ evidence of the defect extent, a phased-array ultrasound system, i.e. DolphiCam, dedicated for NDT inspections on Carbon Fibre Reinforced Polymers (CFRP) materials, was utilized. DolphiCam supports a variety of inspection techniques such as A-, B- and C-Scans. In our test, C-Scan measurements were made utilizing the Time-of-Flight (ToF) feature. The testing operation was paused in several moments in order to perform measurements with the DolphiCam. In Fig. 3a several measurements are presented which progressively capture the fatigue disbond growth of the initial 30-mm rectangle disbond. The disbonded area is graphically enclosed within the black dashed line; the camera measurements

have been made from the skin side of the panel (see Fig. 3b). From the inspection evidence we verify that only after the specimen enters the fatigue loading regime with $P_{max} = -50$ kN, the disbond initiates its propagation along the longitudinal direction. The phased-array inspection was only conducted for specimen L1_22.

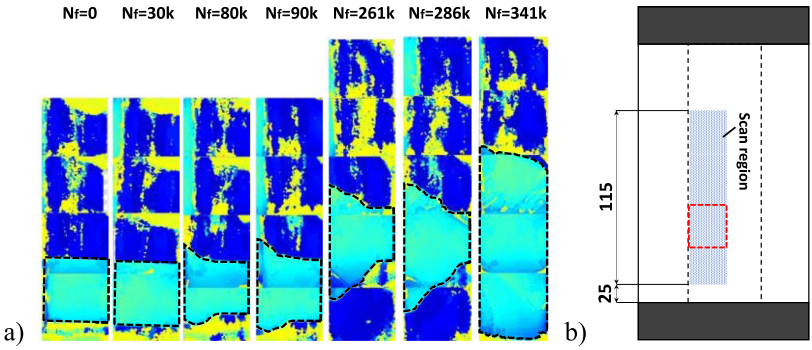

Fig. 3. a) Disbond growth of L1_22 as measured with DolphiCam using ToF feature and b) schematic illustration of the scanned region.

3.3 Strain-Based Health Indicator (HI)

To develop a strain-based HI we face the issue that absolute static strains are strongly dependent on load fluctuations and apparently load does not remain constant during service (see abrupt jumps in Fig. 2a). This means that the strain field might be more influenced by the load than by the defect itself, the latter which is the actual target of the majority of SHM systems. To this end, we proposed in our previous work [15] the following normalization scheme of the FBG strains:

$$(\bar{\varepsilon}_i)_j = \frac{\varepsilon_i}{\frac{1}{n}\sum \varepsilon_i} \tag{3}$$

where, n is the number of FBGs per foot, $i = 1, \ldots, n$ and j is the index that defines the foot, i.e. RF: right foot and LF: left foot ($j = RF, LF$). We have studied the behavior of this normalization scheme in a numerical modeling framework in [15], and observed its dependency, on both load as well as various disbond configurations amidst the skin/stringer interface. The results showed, that prior to buckling this normalization feature presented a stable behavior, whilst when the structure underwent to the post-buckling regime, it deviated from its initial values. This could lead to confusion, as it is likely that the change to the indicator's value is solely attributed to varying loads and not to the actual increase of the disbond. Hence, leveraging on the anti-symmetrical buckling mode shape of the specific test article, the authors proposed the following HI:

$$HI_i = \frac{(\bar{\varepsilon}_i)_{LF} + (\bar{\varepsilon}_i)_{RF}}{2} \tag{4}$$

where *i* stands for the FBG per foot. This indicator now utilizes strains acquired from a pair of sensors that belong to a corresponding position at the two feet of the stiffened panel. The evolution of this HI as well as the normalization schemes are presented in Fig. 4, based on strains acquired from L1_23 at the first QS test, i.e. before the initiation of the fatigue loading, coming from a wide load range [−50, −5] kN. The abscissa of the graphs is expressed in terms of sample points during the QS loading. However, we can clearly identify when buckling occurs by the separation between the two normalized features.

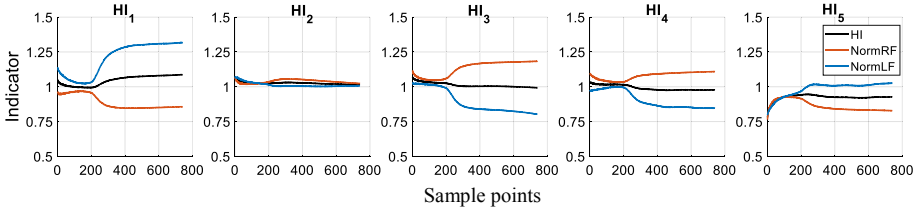

Fig. 4. HIs and normalized strains for all FBGs of L1_23 during the 1st QS loading.

As it can be noticed from Fig. 4, the HI provenly presents a quite stable behavior in an extended load range. So, out of a plethora of values, that correspond to various load magnitudes, we will utilize the arithmetic mean of the HI samples as the monitoring feature. Due to potentially erroneous measurements of sensor R5 in L1_22, the 5th pair of FBGs was excluded from the calculation of the HIs. Out of the acquired data during the QS test, i.e. strains in load range up to P_{max}, a representative sample was created by randomly picking elements from the whole population of strain readings (N_S). Here, the sampling region (N_{SR}) of the randomly selected data will be consisting of 75% of the total sample points (N_S) as highlighted between the two dashed lines in Fig. 5a. In Fig. 5b and Fig. 6 the mean values of the HI samples are presented throughout the test span for specimens L1_23 and L1_22 respectively.

Generally, we can observe monotonic trends on the indicators which is a desirable behavior from a diagnostics as well as a prognostics point of view [16, 17]. However, as the growth of the disbond progressively affects the adjacent sensors, some of the indicators reverse their gradient (also noticed in [15]), like HI_2. This can be attributed to the gradient change of the absolute strain, as for example in sensors R2 of LP_22; when the structure operated with P_{max} = −55 kN, its readings presented consecutive decrease but when P_{max} shifted to −60 kN, in combination with further disbond propagation, the readings of this sensor suddenly increased till final failure. Moreover, two more potential reasons associated with the maximum strain deviation and by extension with the HIs' behavior, can be pointed. Namely, degradation of the overall stiffness of the structure and the FOS's bonding interface, would inevitably affect the strains readings and lead to variation on the values of the HIs during testing.

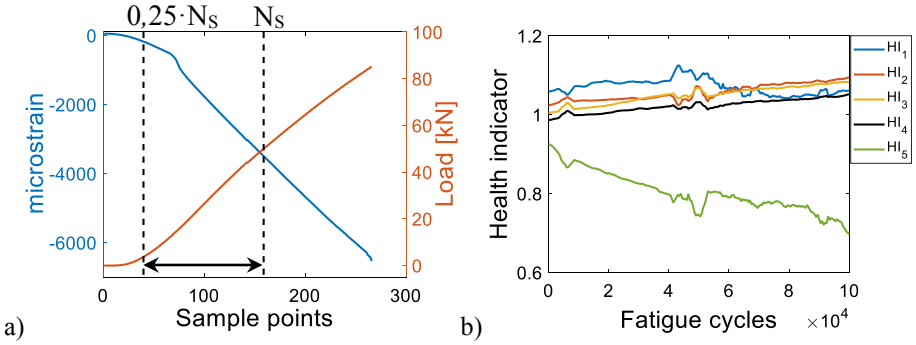

Fig. 5. a) Indicative samples of FBG strain readings and test machine's compressive load, b) evolution of HIs for L1_23.

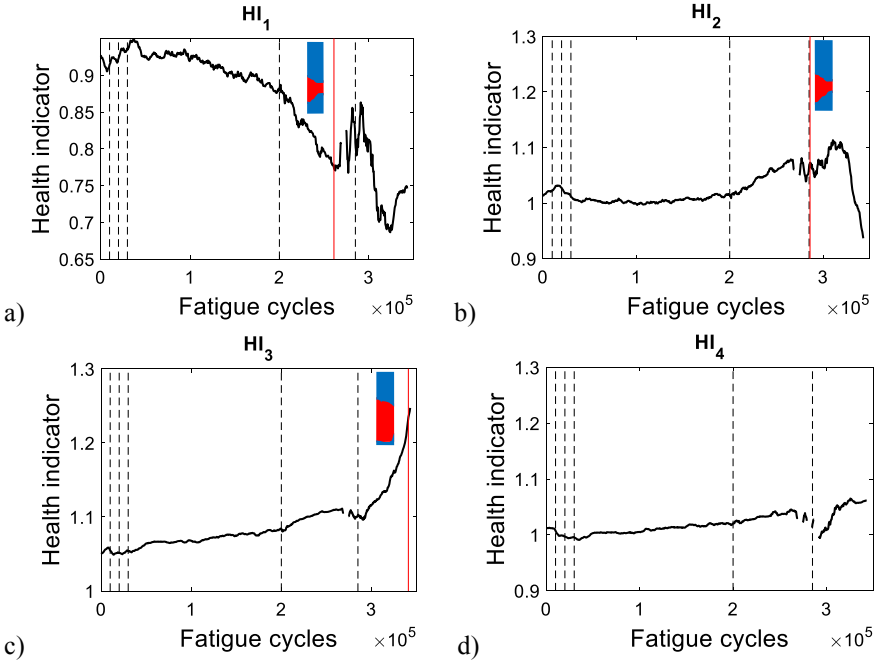

Fig. 6. Evolution of a) HI_1, b) HI_2, c) HI_3 and d) HI_4 for L1_22; black dashed lines represent the change of the block loading limits whilst the red ones indicate the time when the enclosed phased-array scan was made.

4 Conclusions

A strain-based SHM methodology is presented in the current work. Two CFRP single-stiffened panels have been subjected to block loading C-C fatigue. The specimens contained a rectangular artificial disbond in the skin/stringer interface which was

progressively growing due to the fatigue loading. Strain sensing, in terms of surface mounted FBGs, is utilized towards capturing the phenomenon of disbond propagation. NDT inspection, using an ultrasound phased-array camera, provided evidence regarding the morphology of the disbond growth.

The methodology is based on acquiring static strains from the top surface of the stringers' feet. To this direction, a special HI is proposed and assessed as a monitoring feature during the test span. By using the specific HI, we have seemingly achieved to eliminate the abrupt jumps of the absolute strains due to their inherent dependency on load. Moreover, strain data from an extensive load range have been utilized. The HIs' sensitivity to the disbond increase is captured making it a considerable candidate for real-time strain-based feature. Specifically, on specimen L1_22 we report a maximum 25.9%, 8.9% and 15.8% modification on HI_1 (the most affected from the disbond), HI_2 and HI_3 respectively, in comparison to their initial values. HI_4, reflecting on a region where the disbond did not affect the 4^{th} sensor pair, presented a minor modification of 4.6% if compared to its initial value. For L1_23, the most affected indicator, namely HI_5, showed a modification to its values equal to 25.3%, whilst none of the rest HIs presented an overall deviation larger than 7.2%. Also, the present HI proved its ability to maintain its efficiency in cases where some sensors should not be considered, like for the case of sensor R5 of specimen L1_22.

In the future we aim to give further insight in the behavior of this HI, which will be evaluated in an updated test campaign of a random spectrum fatigue excitation assisted by strain sensing during testing. Also, preliminary studies have shown that the HI consistently retains its behavior for various sizes of N_{SR} but an investigation on its proper size will be conducted. Finally, the applicability of this HI to alternative sources of damages, such as impact-induced delaminations, will be investigated.

Acknowledgements. The work was financially supported by the European Union's Horizon 2020 research and innovation programme ReMAP (Grant Agreement Number: 769288).

References

1. Worden, K., Farrar, C.R., Manson, G., Park, G.: The fundamental axioms of structural health monitoring. Proc. R. Soc. A Math. Phys. Eng. Sci. **463**, 1639–1664 (2007)
2. Güemes, A., Fernandez-Lopez, A., Pozo, A.R., Sierra-Pérez, J.: Structural health monitoring for advanced composite structures: a review. J. Compos. Sci. **4**, 13 (2020)
3. Palaniappan, J., et al.: Disbond growth detection in composite-composite single-lap joints using chirped FBG sensors. Compos. Sci. Technol. **68**, 2410–2417 (2008)
4. Pfingstl, S., Steiner, M., Tusch, O., Zimmermann, M.: Crack detection zones: computation and validation. Sens. (Switz.) **20**, 2568 (2020)
5. Sbarufatti, C., Manes, A., Giglio, M.: Performance optimization of a diagnostic system based upon a simulated strain field for fatigue damage characterization. Mech. Syst. Signal Process. **40**, 667–690 (2013)
6. Salvetti, M., et al.: On the performance of a cointegration-based approach for novelty detection in realistic fatigue crack growth scenarios. Mech. Syst. Signal Process. **123**, 84–101 (2019)

7. Dávila, C.G., Bisagni, C.: Fatigue life and damage tolerance of postbuckled composite stiffened structures with initial delamination. Compos. Struct. **161**, 73–84 (2017)
8. Feng, Y., et al.: Effect of fatigue loading on impact damage and buckling/post-buckling behaviors of stiffened composite panels under axial compression. Compos. Struct. **164**, 248–262 (2017)
9. Falzon, B.G., Stevens, K.A., Davies, G.O.: Postbucking behaviour of a blade-stiffened composite panel loaded in uniaxial compression. Compos. Part A Appl. Sci. Manuf. **31**, 459–468 (2000)
10. Yap, J.W.H., Scott, M.L., Thomson, R.S., Hachenberg, D.: The analysis of skin-to-stiffener debonding in composite aerospace structures. Compos. Struct. **57**, 425–435 (2002)
11. Meeks, C., Greenhalgh, E., Falzon, B.G.: Stiffener debonding mechanisms in post-buckled CFRP aerospace panels. Compos. Part A Appl. Sci. Manuf. **36**, 934–946 (2005)
12. Takeda, S., Aoki, Y., Nagao, Y.: Damage monitoring of CFRP stiffened panels under compressive load using FBG sensors. Compos. Struct. **94**, 813–819 (2012)
13. Kolanu, N.R., Raju, G., Ramji, M.: Experimental and numerical studies on the buckling and post-buckling behavior of single blade-stiffened CFRP panels. Compos. Struct. **196**, 135–154 (2018)
14. van den Akker, B.P.H., et al.: The influence of hygrothermal aging on the fatigue behavior and residual strength of post-buckled co-bonded stiffened panels subjected to compressive loading. Compos. Part B Eng. **194**, 108023 (2020)
15. Milanoski, D.P., Loutas, T.H.: Strain-based health indicators for the structural health monitoring of stiffened composite panels. J. Intell. Mater. Syst. Struct. (2020). https://doi.org/10.1177/1045389X20924822
16. Eleftheroglou, N., Loutas, T.: Fatigue damage diagnostics and prognostics of composites utilizing structural health monitoring data and stochastic processes. Struct. Heal. Monit. **15**, 473–488 (2016)
17. Eleftheroglou, N., Zarouchas, D., Loutas, T., Alderliesten, R., Benedictus, R.: Structural health monitoring data fusion for in-situ life prognosis of composite structures. Reliab. Eng. Syst. Saf. **178**, 40–54 (2018)